Article

A Green Route to Copper Loaded Silica Nanoparticles Using Hyperbranched Poly(Ethylene Imine) as a Biomimetic Template: Application in Heterogeneous Catalysis

Dimitris Tsiourvas [1], Aggeliki Papavasiliou [1,*], Evangelia G. Deze [1], Sergios K. Papageorgiou [1], Fotios K. Katsaros [1], George E. Romanos [1], Evangelos Poulakis [2], Constantine J. Philippopoulos [2], Qi Xin [3] and Pegie Cool [3]

[1] Institute of Nanoscience and Nanotechnology, National Center for Scientific Research "Demokritos", Aghia Paraskevi, 153 10 Athens, Greece; d.tsiourvas@inn.demokritos.gr (D.T.); e.deze@inn.demokritos.gr (E.G.D.); s.papageorgiou@inn.demokritos.gr (S.K.P.); f.katsaros@inn.demokritos.gr (F.K.K.); g.romanos@inn.demokritos.gr (G.E.R.)

[2] Chemical Process Engineering Laboratory, Department of Chemical Engineering, National Technical University of Athens, 9 Heroon Polytechniou Str., Zografou Campus, 157 80 Athens, Greece; v.poulakis@gmail.com (E.P.); kphilip@chemeng.ntua.gr (C.J.P.)

[3] Laboratory of Adsorption and Catalysis, Department of Chemistry, University of Antwerpen (CDE), Universiteitsplein 1, 2610 Wilrijk, Belgium; qi.xin@uantwerpen.be (Q.X.); pegie.cool@uantwerpen.be (P.C.)

* Correspondence: a.papavasiliou@inn.demokritos.gr; Tel.: +30-210-650-3913

Abstract: Copper containing silica nanostructures are easily produced through a low cost versatile approach by means of hyperbranched polyethyleneimine (PEI), a water soluble dendritic polymer. This dendritic molecule enables the formation of hybrid organic/inorganic silica nanoparticles in buffered aqueous media, at room temperature and neutral pH, through a biomimetic silicification process. Furthermore, the derived hybrid organic/inorganic materials dispersed in water can be easily loaded with various copper amounts, due to the presence of PEI, which, despite having been integrated in the silica network, retains its strong copper chelating ability. Following calcination, the obtained copper loaded nanopowders are characterized by X-ray diffraction (XRD), Scanning electron microscopy (SEM), N_2 adsorption, Temperature programmed reduction (TPR) and UV-Vis diffuse reflectance (UV-Vis-DR) techniques and evaluated for automotive exhaust purification under simulated conditions at the stoichiometric point. Effective control over final materials' pore structural and morphological characteristics is provided by employing different buffer solutions, i.e., tris(hydroxymethyl)aminomethane (Tris) or phosphate buffer. It was found that the enhancement of the nanopowders textural features, obtained in the presence of Tris buffer, had a great impact on the material's catalytic behavior, improving significantly its activity towards pollutants oxidation.

Keywords: hyperbranched polyethyleneimine; biomimetic synthesis; silica; copper; heterogeneous catalysis

1. Introduction

Over the last few years, dendrimers and hyperbranched polymers, collectively referred to as dendritic polymers, have received great scientific and technological interest, owing to their highly branched tree-like architecture and their multi-functionality [1–5]. Their structure consists of a central point or core from which emanates a network of repeating monomer units and branches, enclosed by terminal functional groups located at the macromolecule's periphery [1–5]. These three structural

components define dendritic polymers' physicochemical characteristics and properties. For example, the ability to encapsulate a large variety of molecules (including catalysts, drug compounds, organic pollutants, etc.) in the nanocavities formed in their interior is strongly dependent on the structural properties of their branches, whereas properties such as solubility, polarity and reactivity with other molecules, molecular aggregates, or substrates, can be easily tuned through modification or functionalization of the terminal groups [2,3]. Compared to dendrimers, hyperbranched polymers possess a less precisely defined chemical architecture, yet still share analogous features and application prospects [3–5]. Their properties, coupled with their facile synthesis, lower cost and greater availability, make them more appealing candidates than their symmetrical analogues [4].

Micelle templating strategy has been used for generating porous materials with high surface area or tunable pore size [6–8]. Lately, dendritic polymers are widely used as nanostructured building blocks in the design of novel nanoarchitectures with potential applications in the fields of catalysis, purification and separation technologies, CO_2 adsorption, biomaterials, electronics, optics, etc. [1–5,9–21]. Due to their pore-templating and structure directing properties, they can produce inorganic matrices with imprinted nanocavities of well-defined size and spheroidal shape [17–21]. There are several synthetic approaches reported in the literature involving condensation reactions, hydrogen-bonding or electrostatic interactions for the assembly of various dendritic molecules into inorganic networks, mostly silica or titania [16–21]. In recent developments, supported-nanoparticle materials are produced by taking advantage of dendritic polymers' dual templating roles. Apart from their ability to act as macromolecular porogens, dendritic polymers can also entrap metal species, affording size-controllable and monodisperse metal or metal oxide nanoparticles, after chemical reduction or thermal treatment [9–14,19–23]. Polymer's generation, number and chemical composition of the peripheral groups as well as stoichiometry of the dendrimer-metal complex are some of the parameters determining final particle size [21–23]. To this direction, our group has employed hyperbranched polyethyleneimine (PEI) for the production of metal loaded silica based catalytic materials [9,10]. PEI is a positively charged water-soluble hyperbranched polymer bearing a large number of peripheral and internal amino groups, which endow a strong chelating action [4,9,10]. The developed synthetic strategies relied on the use of PEI either as a reactive template forming covalent bonds with an appropriate silica precursor or as a secondary structure directing agent applied together with the triblock copolymer Pluronic P123. In both cases, introduction of the desired metal ions (Cu, Ce and Pd) was accomplished through metal-N ligands complex formation.

In addition to the pore-forming and chelating action, another intriguing property of amine terminated dendritic polymers is their ability to activate silica condensation, under environmentally friendly conditions [4,24,25]. It is known that biogenic silica, in nature, is formed through a process known as biosilicification at ambient temperatures, pressures and pH values, affording a large diversity of silica frameworks [26–28]. This process is accredited to polycationic peptides such as the silaffins that are responsible for diatom silicification [26] or to the synthetic peptide analogue R5 [29,30] that, even in vitro, induce the formation of silica nanoparticles within seconds after addition of silicic acid at subsaturating silicic acid concentrations. Likewise, the same property is exhibited by a variety of polycationic synthetic homopeptides, such as poly(arginine) and poly(lysine) [31], as well as by amine-terminated dendrimers [24] or hyperbranched polymers [4]. It was also found that the amine-terminated dendritic polymers yield silica nanoparticles in an amine concentration-dependent manner and that these polymers are entrapped within the growing silica network, as is also the case with the previously described bioactive peptides. Therefore, dendritic molecules can drive biogenic silica nanosphere production evidently due to the highly localized concentration of amino groups. These biomimetic moieties serve as an acid-base catalyst for silica polymerization and concentrate silicate groups at the dendrimer surface, due to electrostatic interactions, further promoting silica condensation reactions and finally yielding composite silica/polymer nanospheres [4,24].

In our previous work, a silicification mimicking process with the use of PEI as a biomimetic template was followed for the generation of hybrid PEI/silica nanopowders in water, under mild

conditions, i.e., ambient temperatures and pressures [4]. Solution pH was regulated at 7.5 with the aid of a phosphate buffer solution. At this pH value, PEI's primary amino-groups are partially protonated in the form of NH_3^+ and electrostatically interact with negatively charged silica species. Through this interaction, PEI's integration within growing silica nanospheres was attained. The developed hybrid nanospheres demonstrated enhanced sorption capacity towards two polycyclic aromatic hydrocarbons and four selected toxic metal ions compared to polymer free nanospheres, confirming the retained chemical and chelating properties of PEI although surrounded by the siloxane network [4].

In the present study, by making use of PEI's biomimetic action and templating properties, copper containing silica nanostructures are developed and examined towards automotive catalytic applications. Two different buffer solutions are employed and their effect on silica's textural and structural properties is investigated. Copper incorporation is performed in a second stage, after the formation of PEI/silica nanospheres, simply by adding the hybrid nanospheres into aqueous copper solutions and allowing Cu sorption to take place. Finally, copper nanoparticles are obtained upon calcination. Potential use of the developed Cu loaded materials in automotive applications is assessed by testing them under simulated exhaust conditions at the stoichiometric point.

2. Results

2.1. Synthesis in Phosphate Buffer (PB)

Initial metal concentrations of aqueous solutions and final metal amounts in the produced solids determined by Energy Dispersive X-ray Spectroscopy (EDX) analysis, are summarized in Table 1. As observed, Cu uptake in the final solids is quite high, ranging from 5.2 to 7.7 wt %, evidencing the preservation of PEI's complex forming properties, even when incorporated into the siliceous matrix. Moreover, hybrid nanospheres' immersion into aqueous copper solution of higher concentration (1000 ppm) resulted in an increased metal content, indicating that initial metal concentration is one of the controlling factors over final metal loading, together with solid/liquid ratio, pH, temperature and total ionic strength of the solution.

Table 1. Samples coding, textural characteristics and final metal loadings.

Samples	Initial Cu Concentration (ppm)	Cu wt %	SSA [1] (m^2/g)	TPV [2] (cm^3/g)
SiO_2_PB	-	-	40	0.14
Cu_5.2 wt %_SiO_2_PB	100	5.2	-	-
Cu_7.7 wt %_SiO_2_PB	1000	7.7	38	0.09
SiO_2_Tris	-	-	557	1.15
Cu_2.4 wt %_SiO_2_Tris	1000	2.4	290	1.02

[1] SSA: specific surface area; [2] TPV: total pore volume.

XRD patterns of the parent and the 7.7 wt % copper loaded silica sample, produced with the aid of a phosphate buffer, are depicted in Figure 1. The metal free sample demonstrates a single very broad diffraction peak at $2\theta \approx 22°$, indicative of the amorphous silica nature, whereas, in the copper loaded one, there is an indication of silica crystallization since the main peak corresponding to tridymite crystal phase could be distinguished. It is highly likely that copper nanocrystallites act as nucleation sites accelerating silica's transition from the amorphous to crystalline phase during the calcination process. This is in agreement with previous studies in which the addition of a small amount of metal ions affected silica's crystallization kinetics [32,33]. Moreover, in the 7.7 wt % copper loaded silica material, trace peaks possibly corresponding to tenorite (JCPDS # 3-884) and copper phosphate (JCPDS # 44-182) phases could also be detected. However, the low intensity broad peaks of Cu crystal phases imply the nanocrystalline nature and the fine dispersion of copper species onto the siliceous support.

Detailed investigation of copper species chemical nature and dispersion state was carried out by means of UV-vis-DR spectroscopy. As noticed in Figure 2, both copper loaded silica samples demonstrate comparable UV-vis spectra. The two bands spotted around 260 nm and 340–360 nm can

be ascribed to charge transfer between mononuclear Cu^{2+} ion and oxygen and between Cu^{2+} and oxygen in oligonuclear $[Cu–O–Cu]_n$ surface species [34,35]. However, the broadness and the intensity of these two bands vary depending on the metal content, revealing a greater contribution of oligomeric copper oxide clusters in the case of the silica sample with the higher copper loading. Bands at higher wavelengths related to the presence of large bulk-like CuO particles [34,35] were not present in any sample examined, supporting the XRD findings.
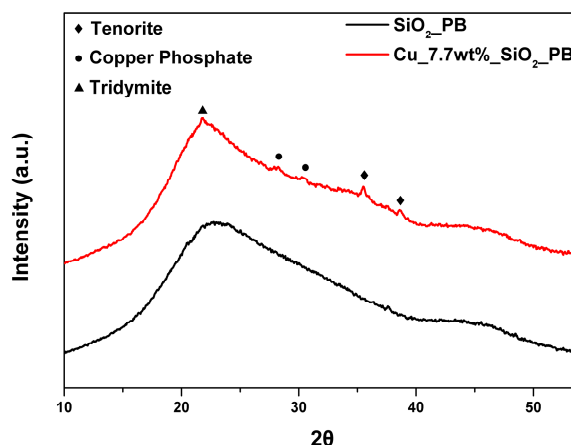

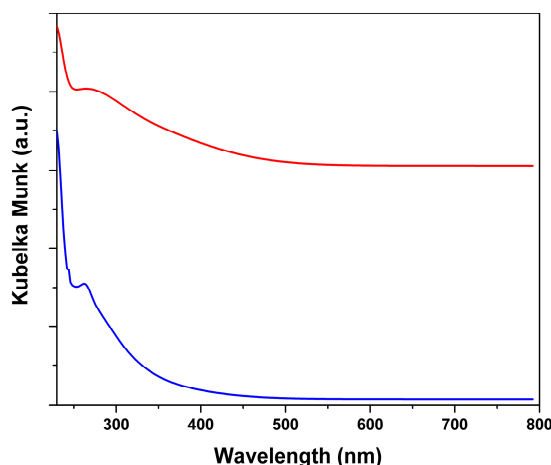**Figure 1.** X-ray diffraction (XRD) patterns of samples produced with phosphate buffer.

Figure 2. UV-Vis diffuse reflectance (UV-Vis-DR) spectra of samples Cu_5.2 wt %_SiO_2_PB (blue line) and Cu_7.7 wt %_SiO_2_PB (red line).

H_2-TPR measurements were performed to probe the reducibility of Cu species onto the siliceous nanospheres. TPR profiles of copper loaded silica samples, along with an unsupported bulk CuO, used as a reference, are illustrated in Figure 3. The sample with the lower copper loading demonstrates a two stage reduction process at 335 °C and 535 °C, with a shoulder at around 300 °C. Taking into consideration the results from UV-vis-DR analysis, where large CuO aggregates could not be identified, these two main peaks may originate from the stepwise reduction of isolated Cu^{2+} species, i.e., $Cu^{2+} \rightarrow Cu^+$ and $Cu^+ \rightarrow Cu^0$ [35,36]. The reduction of copper present in oligomeric oxide clusters accounts for the shoulder observed at lower temperature, since it is well documented in the literature that highly dispersed CuO species are more easily reduced to Cu^0 than isolated Cu^{2+} species [35,36]. The sample with higher metal loading exhibits superior reduction behaviour, with peaks shifted to lower temperature range, as evidenced by the major reduction peak at 280 °C, with a shoulder at 330 °C accompanied by a minor peak at 485 °C. From the position and the intensity of these peaks,

it can be deduced that, in this sample, oligomeric copper oxide clusters are the dominant copper species, in agreement with UV-vis-DR study. Therefore, TPR investigation, together with the findings from UV-vis-DR and XRD analysis, points out the effectiveness of biomimetic synthesis in generating materials with high final metal loading, coupled with an excellent dispersion of the metal species.
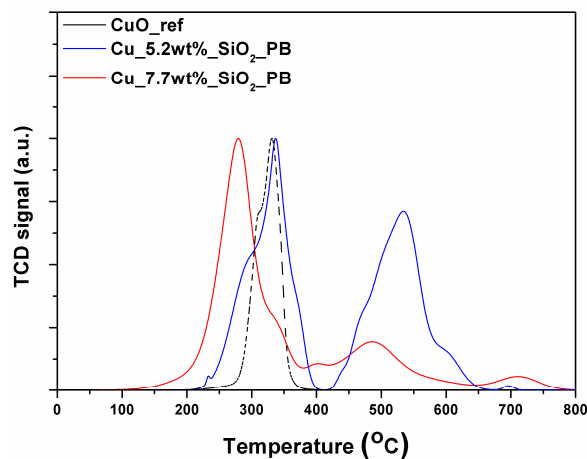

Figure 3. Temperature programmed reduction (TPR) profiles of samples Cu_5.2 wt %_SiO$_2$_PB (blue line), Cu_7.7 wt %_SiO$_2$_PB (red line) and CuO reference (black line).

Morphological characteristics of the as developed materials were assessed by means of SEM microscopy and depicted in Figure 4. As shown, all samples demonstrate the same morphology consisting of well-defined sphere-like particles. The size of the majority of the observed nanospheres ranges between 100 to 300 nm.
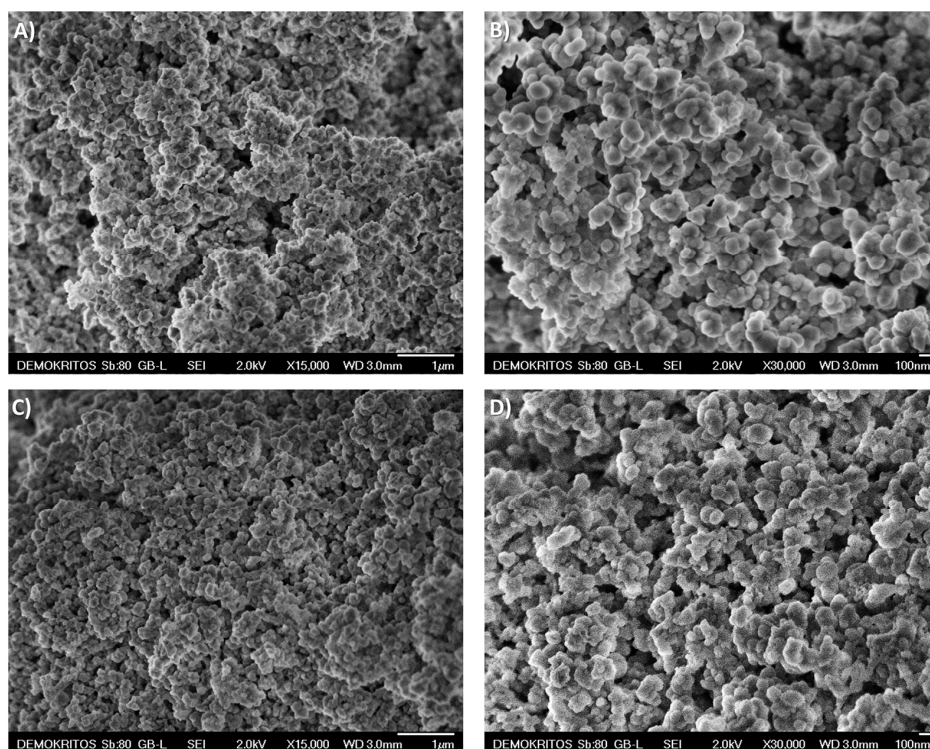

Figure 4. Scanning electron microscopy (SEM) micrographs of samples SiO$_2$_PB (**A**,**B**) and Cu_7.7 wt %_SiO$_2$_PB (**C**,**D**).

Pore structural characteristics, evaluated by N_2 adsorption analysis, are listed in Table 1. Pure silica nanospheres prepared with PB possess very low specific surface area (ssa) and total pore volume (TPV) values, of the order of 40 m^2/g and 0.14 cc/g, respectively. Copper incorporation does not induce drastic changes either in textural features or in isotherm shape. The isotherm plots, illustrated in Figure 5, are of type II with no hysteresis loop, typical of non-porous solids.
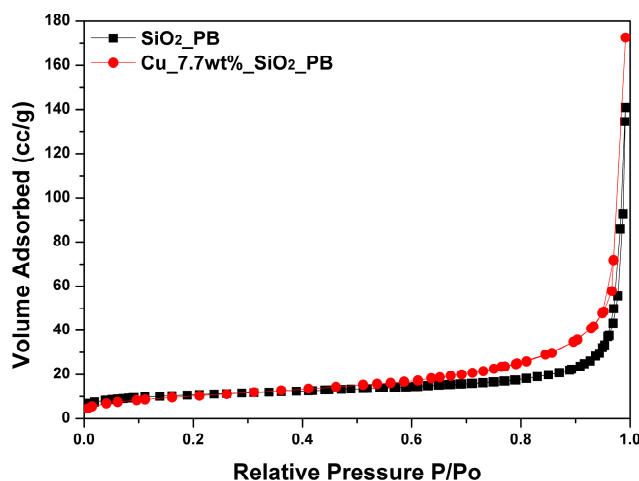

Figure 5. Isotherm plots of samples SiO_2_PB (black line) and Cu_7.7 wt %_SiO_2_PB (red line).

Pollutants' conversion profiles as a function of catalyst temperature, for the sample with the highest Cu loading, are demonstrated in Figure 6. As noticed, this sample is only active towards CO and C_3H_6 oxidation with 31% and 79% maximum conversions achieved at 500 °C, respectively. Concerning the other pollutants, NO, CH_4 and C_3H_8, conversion efficiencies were negligible. This catalytic performance, not in line with the very promising results derived from XRD, UV-vis-DR and TPR analysis, can be attributed to the very poor pore structural characteristics. Bearing in mind the encapsulation of PEI within the growing silica nanospheres, as a result of primary amino moieties multivalency effect [4,9,37], and the preservation of PEI's chelating action even when integrated into the siliceous network [4,9,10], it is anticipated that copper species will be mainly located at the silica's interior and not at the surface. Therefore, the presence of porous channels providing accessibility of reactant gas molecules to the catalytic active sites is of vital importance.
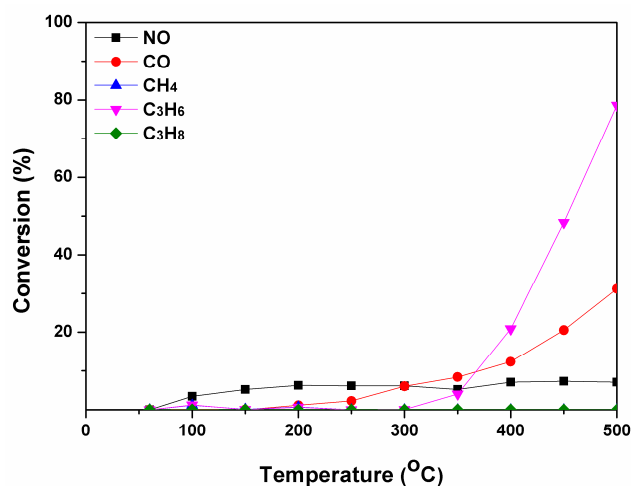

Figure 6. Light-off curves of sample Cu_7.7 wt %_SiO_2_PB.

2.2. Synthesis in Tris Buffer

In order to modify the nanospheres' textural properties and to demonstrate their key role on catalytic behavior, a different buffer solution was employed and examined. The size controlling effect of phosphate buffer solution over biogenic silica nanospheres was reported in a previous work lacking, however, investigation of pore structural properties [25]. Buffer concentration and cation type were recognized as the most crucial factors for particle size control. It was postulated that biomimetic silica growth process is regulated by electrostatic interactions between the negatively charged surface silanol groups and the cations present in solution. As suggested, smaller sized cations, due to the more effective surface coverage and thus charge neutralization, allow particle agglomeration and growth. Larger cations instead lead to insufficient surface coverage, leaving negatively charged silicate surface exposed, thus yielding smaller sized particles, due to the remaining electrostatic repulsions [25]. Prompted by these findings, Tris buffer solution was selected, considering that the cation mediating silica growth is the tris(hydroxymethyl)aminomethane group in its protonated form, which is much larger than the sodium ions present in phosphate buffer.

XRD patterns of pure silica (SiO$_2$_Tris) and the respective copper loaded (Cu_2.4 wt %_SiO$_2$_Tris) samples produced in the presence of Tris buffer solution are shown in Figure 7. In both cases, the only peak detected is the one ascribed to amorphous silica at 2θ ≈ 22°. In the copper loaded sample, the absence of diffractions associated with CuO crystal phase, despite a Cu content of 2.4 wt % (Table 2), implies the very good dispersion of the metal species, not leading to the formation of bulky aggregates detectable by XRD analysis. The lower final copper loading in the presence of Tris compared to phosphate buffer, despite the same initial metal concentration of the employed Cu solution, could be mainly attributed to the lesser incorporation degree of PEI into the formed silica nanospheres.
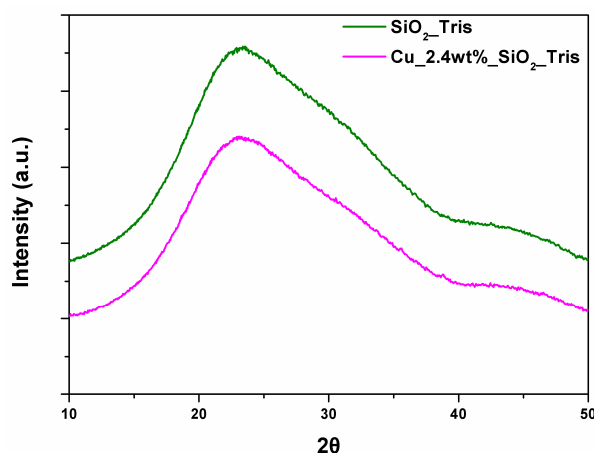

Figure 7. X-ray diffraction (XRD) patterns of samples produced with Tris buffer.

Table 2. Typical composition of car exhaust gases in stoichiometric conditions (λ = 1).

	O$_2$ %	NO ppm	CO %	CH$_4$ ppm	C$_3$H$_6$ ppm	C$_3$H$_8$ ppm	CO$_2$ %	H$_2$ %	H$_2$O %
Λ = 1	0.777	1000	0.7	225	450	225	15	0.233	10

The size controlling effect of the buffer solution is demonstrated by SEM analysis, presented in Figure 8. The developed sample's morphology is notably changed, comprising of much smaller nanospheres (≈30 nm), which form irregular shaped aggregated structures. The use of Tris has also a strong impact on pore structural characteristics, inducing a drastic enhancement in both the ssa (557 m^2/g compared to the 32 m^2/g of SiO$_2$_PB) and pore volume (increase to 1.15 mL/g). Free and copper loaded samples exhibit type IV isotherms Figure 9A, featuring a well-resolved hysteresis loop

corresponding to type H1, characteristic of mesoporous solids. The porous nature of these materials is further manifested by the pore size distribution (PSD), presented in Figure 9B. By inspecting the PSD curves of SiO$_2$_Tris and Cu_2.4 wt %_SiO$_2$_Tris samples, the only difference noticed is the two maxima emerged in the micropore area, which disappeared after metal introduction, evidencing the insertion of copper species within silica's microporous network. Accordingly, a copper loaded sample possesses lower ssa (from 557 to 290 m^2/g) and TPV (from 1.15 to 1.02 mL/g) values, regarding the parent pure silica material.
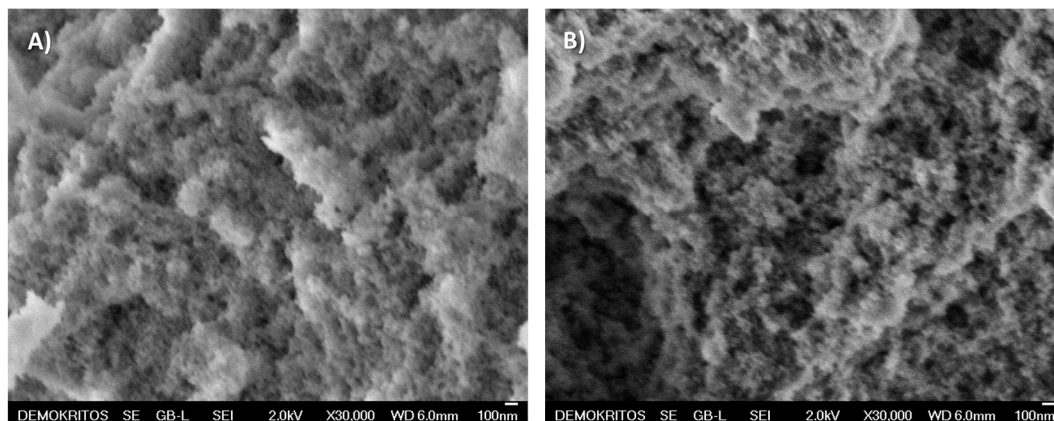

Figure 8. Scanning electron microscopy (SEM) micrographs of samples SiO$_2$_Tris (**A**) and Cu_2.4 wt %_SiO$_2$_Tris (**B**).
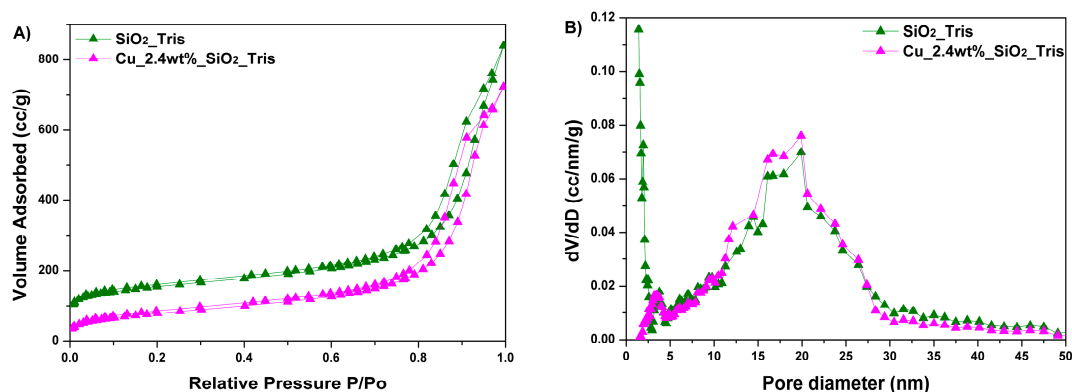

Figure 9. Isotherm plots (**A**) and PSD curves (**B**) of samples produced with Tris buffer.

The aforementioned profound modification of morphological and textural characteristics can be attributed to the larger Tris molecule [25], resulting in insufficient silicate surface coverage yielding smaller sized nanospheres and to its pore forming property, acting as an additional porogen together with PEI. Consequently, catalytic performance was strongly influenced by the use of Tris, despite the lower copper loading. As depicted in Figure 10, the oxidation activity is markedly improved, especially in the case of CO where the maximum conversion reaches up to 80% instead of 31% in the case of phosphate buffer. This is mainly due to the greater accessibility of reactant molecules within the silica porous network facilitating their contact with the catalytic active sites.

To sum up, this work emphasizes the facile fabrication of catalytic systems through a bioinspired route and the investigation of the buffer solution effect on the final material's properties and catalytic behavior. Additionally, catalytic systems with different active phases or even combinations of active compounds can be very easily produced, considering the strong chelating behavior of the employed dendritic polymer for a large variety of metal ions, such as Pt^{2+}, Pd^{2+}, Au^{3+}, Ag$^+$, Cu^{2+}, Ni^{2+}, Ru^{3+}, Mn^{2+} or Fe^{3+}. Therefore, the proposed method represents an effective and versatile technique to

prepare numerous metal loaded silica nanospheres with enhanced catalytic activity. Experiments underway are directed to the incorporation of low Pd amounts into the silica samples, with a view to attain higher three-way catalytic behavior.
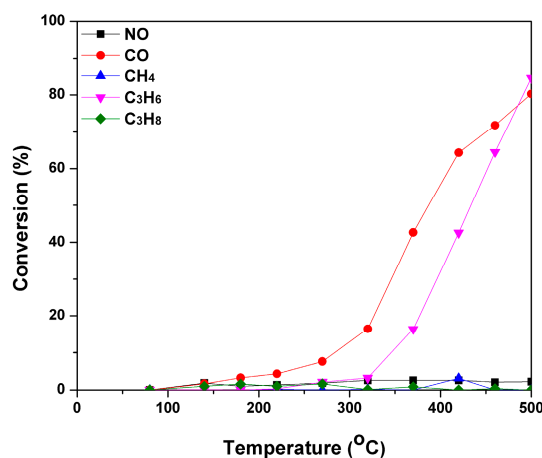

Figure 10. Light-off curves of sample Cu_2.4 wt %_SiO$_2$_Tris.

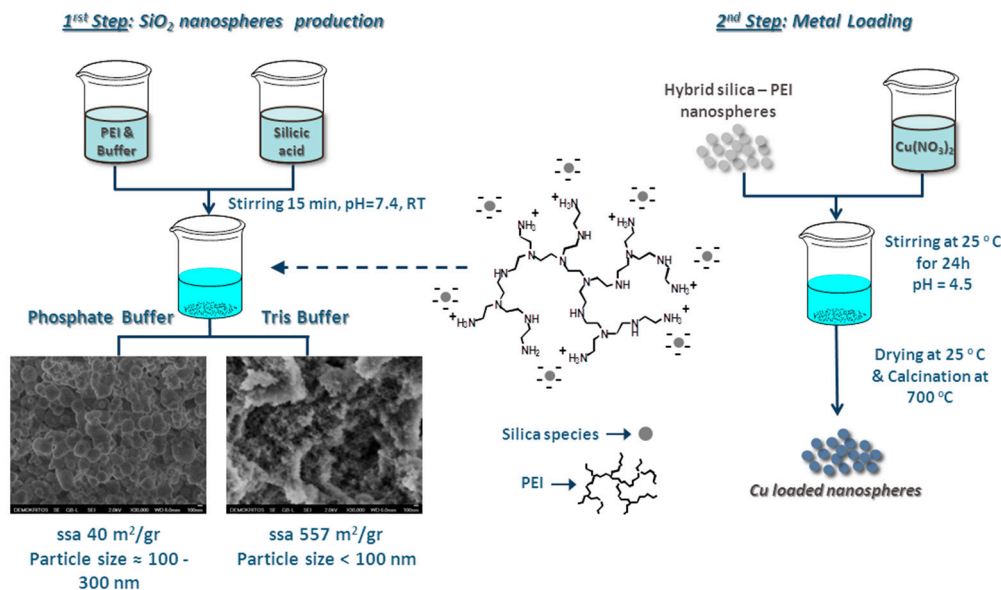## 3. Materials and Methods

3.1. Materials

Hyperbranched poly(ethylene imine), PEI, (BASF, Lupasol G100, Mn = 5000) was kindly donated from BASF (Ludwigshafen, Germany). The primary:secondary:tertiary amino groups ratio was 1:1.10:0.96 as determined employing inverse gated 13C NMR [7].

3.2. Synthesis of Silica/PEI Nanopowders

The preparation of PEI-silica nanoparticles is carried out by following the general procedure described in our previous paper [4]. In short, 1 M silicic acid solution is prepared by the hydrolysis of tetramethyl orthosilicate in 1 mM HCl aqueous media (15 min at room temperature under stirring). This solution (1 mL) is slowly added under vigorous stirring to a PEI buffered solution (10 mL, 20 mM with respect to primary and secondary amine groups). Two different buffer solutions are employed, i.e., a 50 mM, pH 7.4 phosphate buffer (PB) or a 50 mM, pH 7.4 tris(hydroxymethyl)aminomethane (Tris) buffer. The reaction mixtures are allowed under stirring for 15 min and the resulting precipitates are separated by centrifugation at 12,000 rcf for 10 min, washed and centrifuged as above, for a further three times with pure water to ensure complete removal of water soluble species.

3.3. Copper Loading

In a second step, introduction of copper species is carried out through the immersion of a given amount of hybrid silica nanospheres into solutions of different Cu^{2+} concentrations (100 and 1000 ppm at pH 4.5) and stirring at RT for 24 h, in order to obtain Cu^{2+}-PEI complexes. The solid samples, after centrifugation, are thoroughly washed with distilled H$_2$O to remove uncomplexed Cu^{2+} and dried overnight at 50 °C. Finally, calcination at 700 °C for 3 h under airflow (100 mL min^{-1}) and a heating rate of 3 °C/min is performed in a tube furnace, for the removal of the organic template and the acquisition of the catalytic material. The overall synthetic procedure is illustrated in Scheme 1.

Scheme 1. Synthesis of Cu/SiO$_2$ nanospheres through biomimetic approach.

3.4. Characterization Techniques

Copper loadings were determined by EDX analysis on a JEOL JXA 733 (AXES UA) (JEOL Ltd., Tokyo, Japan). Samples were grinded and dispersed on a copper grid coated with a carbon film. N$_2$ adsorption isotherms were collected at 77 K on an automated volumetric system (AUTOSORB-1-Krypton version—Quantachrome Instruments, Boynton Beach, FL, USA). Prior to the measurements, the samples were outgassed at 250 °C for 24 h. Specific surface area was determined using the Brunauer–Emmett–Teller (BET) method. The pore size distribution was calculated using the Nonlocal Density Functional Theory (NLDFT) model (Quantachrome Instruments, AS1Win, Version 2.01, 2016, DFT software). Data reduction parameters: Calc. Model: N$_2$ at 77 K on silica (cylindrical pore, NLDFT equilibrium model). Scanning Electron Microscopy analysis was conducted with a field emission scanning electron microscope (JSM 7401F, JEOL Ltd., Tokyo, Japan), equipped with Gentle Beam mode. XRD diffraction patterns were acquired using a Rigaku rotating anode X-ray generator (operating at 50 kV, 100 mA, nickel-filtered CuKa1 radiation) and an R-AXIS IV image plate (Rigaku Co., Tokyo, Japan). Samples were sealed in Lindemann capillaries. UV-visible diffuse reflectance (UV-vis-DR) analysis was carried out on a Nicolet Evolution 500 spectrophotometer (Thermo Electron Corporation, Waltham, MA, USA). The spectra were obtained in the range of 200–800 nm and the samples were diluted in KBr (2 wt %). Temperature programmed reduction measurements of the catalysts were performed in a Quantachrome iQ. About 50 mg of the sample was outgassed at 473 K for 16 h. After cooling, the sample was first pretreated at 523 K under a He flow for 1 h and then samples were reduced with 5% H$_2$/Ar at a flow rate of 25 mL/min and the temperature was increased from 313 K to 1073 K at 10 K/min. The hydrogen consumption was continuously monitored using a thermal conductivity detector (TCD).

3.5. Catalytic Activity Measurements

Catalytic samples (200 mg) were placed in the middle of a stainless steel tube reactor of 7 mm inner diameter, with quartz wool added at both sides. The reactor was fitted inside a temperature controlled furnace and the catalyst temperature was continuously monitored by two thermocouples situated on the outer side of the reactor, before and after the catalyst. In an effort to better simulate real exhaust conditions, the experimental protocol followed for the acquisition of activity measurements involves a complex feed stream containing 10% H$_2$O, CO$_2$ and a mixture of hydrocarbons (CH$_4$, C$_3$H$_8$ and C$_3$H$_6$). The gas mixture feed was prepared from the following six gas cylinders: 2000 ppm NO and N$_2$

(balance), air, N_2, CO, and a mixture of 0.15% CH_4, 0.15% C_3H_8, 0.28% C_3H_6, 1.59% H_2 and N_2 (balance). The volumetric flow of each stream was controlled by thermal mass flows (Brooks Instrument, Hatfield, PA, USA) and a total feed similar to the typical composition of car exhaust gases at stoichiometric conditions was prepared (Table 2). The total volumetric flow was set to 200 NmL/min in order to correspond to 60,000 h^{-1} space velocity. The addition of 10% H_2O was obtained by passing the feed through a thermostated water bubbler. In the outlet stream, hydrocarbon concentrations were monitored by gas chromatography (Shimadzu GCe17A, column HP PlotQ, FID detector, Kyoto, Japan), NO/NO_2 concentrations by a chemiluminescence analyzer (Model 42-HL, Thermo Scientific, Waltham, MA, USA) and CO concentration by an electrochemical detector (Dräger X-am® 7000, Lübeck, Germany). To ensure stable operation of the catalytic materials, before the evaluation of the catalytic activity, samples were treated with gas feed in stoichiometric composition (50 NmL/min total volumetric flow). The temperature ramp was set to 20–500 °C with 8 °C/min rate and remained at 500 °C for 2 h. The activity tests were performed between 50 to 500 °C and conversion performance was recorded every 50 °C.

4. Conclusions

In the present study, hyperbranched polyethylenemine (PEI), a low cost positively charged dendritic macromolecule is employed both as a biomimetic template and metal binding agent, for the synthesis of copper containing silica nanostructures, and tested for a gasoline engine three-way application. The proposed synthetic route is of particular interest, given that it is a facile, non-energy demanding, cost-efficient, environmentally friendly and versatile method and can therefore be easily adapted for large-scale industrial applications. Formation of PEI/silica nanospheres is initiated in the first step by the electrostatic interactions between PEI's protonated primary amino moieties and negatively charged silica species. PEI's encapsulation within the growing nanospheres enables the easy production of the final copper loaded silica materials, in a second step, by impregnation of the as-developed nanospheres into aqueous copper solutions. As demonstrated by EDX, XRD and UV-Vis-DR analysis, PEI's chelating action affords silica with high copper loading, combined with excellent dispersion. However, the lack of porosity in the as-developed materials has a strong impact on the catalytic performance. Tuning of silica nanospheres' morphological and textural features was attained by employing different buffer solutions. The two buffers examined are a phosphate buffer and Tris, with the latter affording smaller sized nanospheres possessing enhanced textural properties, as a result of insufficient silica surface charge neutralization and Tris's pore forming properties. This modification in the material's nanoporous network, induced by Tris buffer, produced a marked improvement in oxidation activity (i.e., 2.5 higher CO conversion efficiency with lower copper loading), demonstrating a strong correlation between catalytic performance and textural properties.

Author Contributions: Dimitris Tsiourvas, Aggeliki Papavasiliou and Fotios K. Katsaros conceived and designed the experiments; Dimitris Tsiourvas and Aggeliki Papavasiliou performed the experiments; Qi Xin, Pegie Cool and Evangelia G. Deze performed the EDX, TPR and UV-vis-DR techniques; Constantine J. Philippopoulos and Evangelos Poulakis performed the catalytic performance tests; Aggeliki Papavasiliou and George E. Romanos analyzed the data; Aggeliki Papavasiliou wrote the paper; Fotios K. Katsaros, Sergios K. Papageorgiou and George E. Romanos revised and modified the paper.

Conflicts of Interest: The authors declare no conflict of interest.

References

1. Gao, C.; Yan, D. Hyperbranched polymers: From synthesis to applications. *Prog. Polym. Sci.* **2004**, *29*, 183–275. [CrossRef]
2. Tomalia, D.A. Birth of a new macromolecular architecture: Dendrimers as quantized building blocks for nanoscale synthetic polymer chemistry. *Prog. Polym. Sci.* **2005**, *30*, 294–324. [CrossRef]

3. Arkas, M.; Tsiourvas, D.; Paleos, C.M. Functional Dendritic Polymers for the Development of Hybrid Materials for Water Purification. *Macromol. Mater. Eng.* **2010**, *295*, 883–898. [CrossRef]

4. Arkas, M.; Tsiourvas, D. Organic/inorganic hybrid nanospheres based on hyperbranched poly(ethylene imine) encapsulated into silica for the sorption of toxic metal ions and polycyclic aromatic hydrocarbons from water. *J. Hazard. Mater.* **2009**, *170*, 35–42. [CrossRef] [PubMed]

5. Arkas, M.; Eleades, L.; Paleos, C.M.; Tsiourvas, D. Alkylated Hyperbranched Polymers as Molecular Nanosponges for the Purification of Water from Polycyclic Aromatic Hydrocarbons. *J. Appl. Polym. Sci.* **2005**, *97*, 2299–2305. [CrossRef]

6. Bhaway, S.M.; Qiang, Z.; Xia, Y.; Xia, X.; Lee, B.; Yager, K.G.; Zhang, L.; Kisslinger, K.; Chen, Y.-M.; Liu, K.; et al. Operando Grazing Incidence Small-Angle X-ray Scattering/X-ray Diffraction of Model Ordered Mesoporous Lithium-Ion Battery Anodes. *ACS Nano* **2017**, *11*, 1443–1454. [CrossRef] [PubMed]

7. Wang, S.; Tangvijitsaku, P.; Qiang, Z.; Bhaway, S.M.; Lin, K.; Cavicchi, K.A.; Soucek, M.D.; Vogt, B.D. Role of Amphiphilic Block Copolymer Composition on Pore Characteristics of Micelle-Templated Mesoporous Cobalt Oxide Films. *Langmuir* **2016**, *32*, 4077–4085. [CrossRef] [PubMed]

8. Qiang, Z.; Guo, Y.; Liu, H.; Cheng, S.Z.D.; Cakmak, M.; Cavicchi, K.A.; Vogt, B.D. Large-Scale Roll-to-Roll Fabrication of Ordered Mesoporous Materials using Resol-Assisted Cooperative Assembly. *ACS Appl. Mater. Interfaces* **2015**, *7*, 4306–4310. [CrossRef] [PubMed]

9. Deze, E.G.; Papavasiliou, A.; Papageorgiou, S.K.; Katsaros, F.K.; Kouvelos, E.P.; Romanos, G.E.; Boukos, N.; Xin, Q.; Nyalosaso, J.L.; Cool, P. Metal loaded nanoporous silicas with tailor-made properties through hyperbranched polymer assisted templating approaches. *Microporous Mesoporous Mater.* **2016**, *235*, 107–119. [CrossRef]

10. Papavasiliou, A.; Tsiourvas, D.; Deze, E.G.; Papageorgiou, S.K.; Katsaros, F.K.; Poulakis, E.; Philippopoulos, C.J.; Boukos, N.; Xin, Q.; Cool, P. Hyperbranched polyethyleneimine towards the development of homogeneous and highly porous CuO–CeO_2–SiO_2 catalytic materials. *Chem. Eng. J.* **2016**, *300*, 343–357. [CrossRef]

11. Liu, Y.; Dai, J.; Xu, L.; Liu, X.; Liu, J.; Li, G. Red to brown to green colorimetric detection of Ag^+ based on the formation of Au-Ag core-shell NPs stabilized by a multi-sulfhydryl functionalized hyperbranched polymer. *Sens. Actuators B* **2016**, *237*, 216–223. [CrossRef]

12. Knecht, M.R.; Garcia-Martinez, J.C.; Crooks, R.M. Synthesis, Characterization, and Magnetic Properties of Dendrimer-Encapsulated Nickel Nanoparticles Containing <150 Atoms. *Chem. Mater.* **2006**, *18*, 5039–5044. [CrossRef]

13. Albiter, M.A.; Morales, R.; Zaera, F. Dendrimer-based synthesis of Pt catalysts for hydrocarbon conversion. *Appl. Catal. A Gen.* **2011**, *391*, 386–393. [CrossRef]

14. Myers, V.S.; Weir, M.G.; Carino, E.V.; Yancey, D.F.; Pande, S.; Crooks, R.M. Dendrimer-encapsulated nanoparticles: New synthetic and characterization methods and catalytic applications. *Chem. Sci.* **2011**, *2*, 1632–1646. [CrossRef]

15. Tsoufis, T.; Katsaros, F.; Sideratou, Z.; Kooi, B.J.; Karakassides, M.A.; Siozios, A. Intercalation Study of Low-Molecular-Weight Hyperbranched Polyethyleneimine into Graphite Oxide. *Chem. A Eur. J.* **2014**, *20*, 8129–8137. [CrossRef] [PubMed]

16. Kriesel, J.W.; Tilley, T.D. Synthesis and Chemical Functionalization of High Surface Area Dendrimer-Based Xerogels and Their Use as New Catalyst Supports. *Chem. Mater.* **2000**, *12*, 1171–1179. [CrossRef]

17. Rogers, M.C.; Adisa, B.; Bruce, D.A. Synthesis and characterization of dendrimer-templated mesoporous oxidation catalysts. *Catal. Lett.* **2004**, *98*, 29–36. [CrossRef]

18. Volden, S.; Glomm, W.R.; Magnusson, H.; Øye, G.; Sjoblom, J. Dendrimers and Hyperbranched Polyesters as Structure-Directing Agents in the Formation of Nanoporous Silica. *J. Dispers. Sci. Technol.* **2006**, *27*, 893–897. [CrossRef]

19. Larsen, G.; Noriega, S. Dendrimer-mediated formation of Cu–CuO_x nanoparticles on silica and their physical and catalytic characterization. *Appl. Catal. A Gen.* **2004**, *278*, 73–81. [CrossRef]

20. Velarde-Ortiz, R.; Larsen, G. A Poly(propylene imine) (DAB-Am-64) Dendrimer as Cu^{2+} Chelator for the Synthesis of Copper Oxide Clusters Embedded in Sol-Gel Derived Matrixes. *Chem. Mater.* **2002**, *14*, 858–866. [CrossRef]

21. Scott, R.W.J.; Wilson, O.M.; Crooks, R.M. Titania-Supported Au and Pd Composites Synthesized from Dendrimer-Encapsulated Metal Nanoparticle Precursors. *Chem. Mater.* **2004**, *16*, 5682–5688. [CrossRef]

22. Niu, Y.; Crooks, R.M. Dendrimer-encapsulated metal nanoparticles and their applications to catalysis. *C. R. Chim.* **2003**, *6*, 1049–1059. [CrossRef]

23. Lomnicki, S.M.; Wu, H.; Osborne, S.N.; Pruett, J.M.; McCarley, R.L.; Poliakoff, E.; Dellinger, B. Size-selective synthesis of immobilized copper oxide nanoclusters on silica. *Mater. Sci. Eng. B* **2010**, *175*, 136–142. [CrossRef] [PubMed]

24. Knecht, M.R.; Wright, D.W. Amine-Terminated Dendrimers as Biomimetic Templates for Silica Nanosphere Formation. *Langmuir* **2004**, *20*, 4728–4732. [CrossRef] [PubMed]

25. Knecht, M.R.; Sewell, S.L.; Wright, D.W. Size Control of Dendrimer-Templated Silica. *Langmuir* **2005**, *21*, 2058–2061. [CrossRef] [PubMed]

26. Kroger, N.; Deutzman, R.; Sumper, M. Polycationic peptides from diatom biosilica that direct silica nanosphere formation. *Science* **1999**, *286*, 1129–1132. [PubMed]

27. Kroger, N.; Deutzman, R.; Bergsdorf, C.; Sumper, M. Species-specific polyamines from diatoms control silica morphology. *Proc. Natl. Acad. Sci. USA* **2000**, *97*, 14133–14138. [CrossRef] [PubMed]

28. Sumper, M.; Brunner, E. Learning from diatoms: Nature's tools for the production of nanostructured silica. *Adv. Funct. Mater.* **2006**, *16*, 17–26. [CrossRef]

29. Knecht, M.R.; Wright, D.W. Functional analysis of the biomimetic silica precipitating activity of the R5 peptide from *Cylindrotheca fusiformis*. *Chem. Commun.* **2003**, *24*, 3038–3039. [CrossRef]

30. Senior, L.; Crump, M.P.; Williams, C.; Booth, P.J.; Mann, S.; Perriman, A.W.; Curnow, P. Curnow Structure and function of the silicifying peptide R5. *J. Mater. Chem. B* **2015**, *3*, 2607–2614. [CrossRef]

31. Coradin, T.; Durupthy, O.; Livage, J. Interactions of amino-containing peptides with sodium silicate and colloidal silica: A biomimetic approach of silicification. *Langmuir* **2002**, *18*, 2331–2336. [CrossRef]

32. Williamson, J. The Kinetics of Crystal Growth in an Aluminosilicate Glass Containing Small Amounts of Transition-metal Ions. *Mineral. Mag.* **1970**, *37*, 759–770. [CrossRef]

33. Pol, V.G.; Gedanken, A.; Calderon-Moreno, J. Deposition of Gold Nanoparticles on Silica Spheres: A Sonochemical Approach. *Chem. Mater.* **2003**, *15*, 1111–1118. [CrossRef]

34. Praliaud, H.; Mikhailenko, S.; Chajar, Z.; Primet, M. Surface and bulk properties of Cu–ZSM-5 and Cu/Al$_2$O$_3$ solids during redox treatments. Correlation with the selective reduction of nitric oxide by hydrocarbons. *Appl. Catal. B Environ.* **1998**, *16*, 359–374. [CrossRef]

35. Chmielarz, L.; Kustrowski, P.; Dziembaj, R.; Cool, P.; Vansant, E.F. SBA-15 mesoporous silica modified with metal oxides by MDD method in the role of DeNO$_x$ catalysts. *Microporous Mesoporous Mater.* **2010**, *127*, 133–141. [CrossRef]

36. Patel, A.; Shukla, P.; Rufford, T.; Wang, S.; Chen, J.; Rudolph, V.; Zhu, Z. Catalytic reduction of NO by CO over copper-oxide supported mesoporous silica. *Appl. Catal. A Gen.* **2011**, *409–410*, 55–65. [CrossRef]

37. Paleos, C.M.; Tsiourvas, D.; Sideratou, Z.; Tziveleka, L.A. Drug delivery using multifunctional dendrimers and hyperbranched polymers. *Expert Opin. Drug Deliv.* **2010**, *7*, 1387–1398. [CrossRef] [PubMed]